DIGITAL TRANSMITTER I/Q IMBALANCE CALIBRATION: REAL-TIME PROTOTYPE IMPLEMENTATION AND PERFORMANCE MEASUREMENT

Olli Mylläri, Lauri Anttila, and Mikko Valkama

Department of Communications Engineering, Tampere University of Technology
P.O.Box 553, FI-33101 Tampere, Finland
phone: + (358) 3 311 511, fax: + (358) 3 311 538 08, email: {olli.myllari, lauri.anttila, mikko.e.valkama}@tut.fi

ABSTRACT

Nowadays, the direct-conversion and the low-IF transceiver principles are seen as the most promising architectures for future flexible radios. Both of the architectures employ complex I/Q mixing for up- and downconversion. Consequently, the performance of the transceiver architectures can be seriously deteriorated by the phenomenon called I/Q imbalance. I/Q imbalance stems from relative amplitude and phase mismatch between I- and Q-branches of the transceiver. As a result, self-interference or adjacent channel interference is introduced. This paper addresses details of the real-time prototype implementation of the transceiver unit realizing widely-linear least-squares based I/Q imbalance estimation algorithm and corresponding pre-distortion structure proposed earlier by the authors. First the estimation itself is reviewed and a recursive version of it is derived. After that, implementation related practical issues are addressed and implementation platform is also briefly introduced. Finally, implementation details and comprehensive RF measurement results from the real-time implementation are presented.

1. INTRODUCTION

The current trend in implementing future wireless radio transceivers is to use the direct-conversion or the low-IF transceiver architectures [1, 2]. However, there are still number of practical issues to be overcome before these transceiver architectures can be fully implemented in future wideband flexible transceiver units. In both architectures many transceiver functions have been moved from analog parts towards the digital signal processing (DSP) parts, thus enabling low-cost, simple, less power consuming and highly integrable transceiver unit [2]. One practical problem, however, is the sensitivity of such simplified analog front-ends (FE) to imperfections of the used radio electronics. This is the central theme also in this article, with most focus on the transmitter (TX) side.

Both of the above transceiver architectures are based on analog complex in-phase/quadrature (I/Q) up- and downconversion which makes them vulnerable to amplitude and phase mismatch between I- and Q-branches. As a result, there is crosstalk between mirror frequencies which yields, depending on the selected transceiver architecture, self-interference or adjacent channels interference, when interpreted in frequency domain. Other major nonidealities on TX side are local oscillator (LO) leakage and power amplifier (PA) nonlinearity which also contribute to signal deterioration [3]. Moreover, future wireless systems demand higher transmission rates which yields wider bandwidths, higher order modulations and utilization of multi carrier schemes. However, signals with wider bandwidths and higher order modulations, and multi-carrier (MC) signals (e.g. OFDM) are especially sensitive to analog FE nonidealities [3, 4].

This paper focuses to implementations related details and practical aspects of TX I/Q imbalance calibration scheme based on parameter estimation by widely-linear least-squares (WL-LS) approach and pre-distortion (PD) filtering. Special emphasis is on real-time prototype implementation and RF performance measurements of a complete TX. The approach here is applicable for single-carrier (SC) and MC signals.

The paper is organized as follows. First in Section 2 I/Q imbalance as a phenomenon and TX signal model are introduced, and selected PD structure is reviewed. Thereafter in Section 3, recursive WL-LS approach-based I/Q imbalance parameter estimation is derived. Then implementation related problems are discussed in Section 4. After that, the implementation platform is introduced in Section 5. After that, implementation details and measurement results are presented and analyzed in Section 6. Paper is concluded in Section 7.

Notation: $(.)^*$ denotes complex conjugation, $(.)^H$ hermitian transpose and $*$ convolution. All bold lower-case letters and upper-case letters denote vectors and matrices, respectively.

2. I/Q IMBALANCE AND DIGITAL PRE-DISTORTER STRUCTURE

In an ideal I/Q TX, analog circuits in the I and Q branches have equal characteristics, but in practice, due to hardware manufacturing tolerances a perfectly balanced analog FE is not achievable. In addition, electrical characteristics of analog components can undergo short time deviation due to e.g. temperature variation and, similarly, they are subjected to change over long time period due to aging. These physical limitations in the implementation accuracy of analog I/Q processing result in a finite attenuation of the image frequencies and thus degrades the transmit signal quality. Current state-of-the-art transceivers have around $1-2\%$ amplitude imbalance and $1-2^\circ$ phase imbalance which yields about $30-40$dB image rejection ratio (IRR) [2].

The approach in this paper to overcome I/Q imbalance problem is to use DSP techniques to compensate the I/Q imbalance effects. The DSP based calibration methods allow errors in the analog design and have an advantage of achieving good performance without modifying the original transceiver architecture. In addition, adaptive DSP based approaches enable the possibility to follow time-variant changes of the TX FE.

2.1 Signal Model

In a wideband system context, the overall effective I/Q imbalance effects can vary as a function of frequency over the whole frequency band and wider bandwidths are more vulnerable to the frequency-selective behavior of I/Q imbalance [5]. Consequently, the I/Q imbalance can be modeled as frequency-selective relative amplitude and phase difference between the I and Q branches. In following, g_T and ϕ_T are the I/Q mixer amplitude and phase imbalances, respectively. In addition, the non-ideal filter characteristics between the I and Q branches is modeled with the filters $h_I(t)$ and $h_Q(t)$. If signal bandwidth is narrow, the imbalance model is considered to be frequency-independent and the filters $h_I(t)$ and $h_Q(t)$ can be extracted from the formulation.

For further analysis, denote the ideal baseband equivalent transmit signal as $z(t) = z_I(t) + jz_Q(t)$. The corresponding imbalanced baseband equivalent is then [6]

$$x(t) = g_1(t) * z(t) + g_2(t) * z^*(t). \quad (1)$$

With further derivation the impulse responses $g_1(t)$ and $g_2(t)$ can be shown to be $g_1(t) = [h_I(t) + g_T exp(j\phi_T) h_Q(t)]/2$ and $g_2(t) = [h_I(t) - g_T exp(j\phi_T) h_Q(t)]/2$ [7]. In addition, the Fourier transform

 ISSN 2076-1465

(FT) of $x(t)$ is $X(f) = G_1(f)Z(f) + G_2(f)Z^*(-f)$. From $X(f)$ the mirror frequency attenuation can be found to be

$$IRR_{dB}(f) = 10\log_{10}\left(\frac{|G_1(f)|^2}{|G_2(f)|^2}\right). \quad (2)$$

2.2 I/Q Imbalance Compensation

The aim of the I/Q imbalance mitigation is to remove conjugate term in (1) by properly pre-distorting the ideal TX data. Based on above imbalance model, and switching to discrete-time notations, the following PD of the form

$$z_p(n) = z(n) + w(n) * z^*(n) \quad (3)$$

can be used [7]. Here $w(n)$ represents the PD impulse response. From (1) and (3), it follows that the pre-distorted and imbalanced signal is $x_p(n) = g_{1,p}(n) * z(n) + g_{2,p}(n) * z^*(n)$, where the modified imbalance model impulse responses are $g_{1,p}(n) = g_2(n) + g_1(n) * w^*(n)$ and $g_{2,p}(n) = g_2(n) + g_1(n) * w(n)$. From this it can be derived that optimum solution for PD must satisfy $g_{2,p}(n) = g_2(n) + g_1(n) * w(n) = 0, \forall n$. Solution can be seen more intuitively after FT, as

$$W_{OPT}(e^{j\omega}) = \frac{-G_2(e^{j\omega})}{G_1(e^{j\omega})}, \quad (4)$$

where ω is normalized angular frequency. In practice, however, this solution cannot be directly used for estimation because $g_1(n)$ and $g_2(n)$ are considered unknown. Thus, practical imbalance parameter estimation schemes using feedback from RF back to TX digital parts are addressed next.

The PD structure realizing above derivation can be seen in Fig. 1. In the figure, after the real mixing, filtering and ADC, the DSP block performs final down-conversion from the IF to baseband and consequent decimation and low-pass filtering. Moreover, DC offset removal, timing synchronization, I/Q imbalance parameter estimation and PD filter calculation are performed inside the DSP block. Here, real mixing is chosen to avoid any additional I/Q imbalance to the feedback loop (FBL) signal.

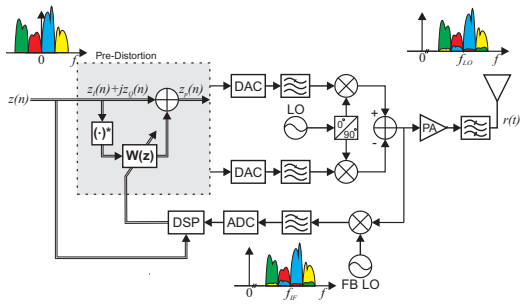

Figure 1: Block diagram I/Q up-conversion based TX structure with calibration functionality.

3. I/Q IMBALANCE PARAMETER ESTIMATION

In this section the WL-LS estimation method described in [7] is briefly reviewed and derivation of recursive version of it is introduced being particularly suitable for real-time implementations. Imbalance parameter estimation is in general based on a feedback signal capturing the complex envelope of the generated RF waveform back to the TX digital parts. This is illustrated in Fig. 1.

From now on, switching to vector-matrix notation for convenience. First, derive an estimator for $\tilde{\mathbf{g}}_1$ and $\tilde{\mathbf{g}}_2$, which include also FBL response, using time-domain model-fitting approach. The aim is to find estimates $\hat{\mathbf{g}}_1$ and $\hat{\mathbf{g}}_2$ which give the best fit between original data sequence $\mathbf{z}(n)$ and observed feedback data sequence $\mathbf{y}(n)$.

3.1 Block Least-Squares Approach

After removing FBL delay the observed feedback data sequence can be formulated as

$$\begin{aligned}\mathbf{y}(n) &= \mathbf{Z}(n)\hat{\mathbf{g}}_1 + \mathbf{Z}^*(n)\hat{\mathbf{g}}_2 \\ &= [\mathbf{Z}(n)\ \mathbf{Z}^*(n)]\begin{bmatrix}\hat{\mathbf{g}}_1 \\ \hat{\mathbf{g}}_2\end{bmatrix} \\ &= \mathbf{Z}_b(n)\begin{bmatrix}\hat{\mathbf{g}}_1 \\ \hat{\mathbf{g}}_2\end{bmatrix},\end{aligned} \quad (5)$$

where $\mathbf{y}(n) = [y(n)\ y(n-1)\ \cdots\ y(n-L_b+1)]^T$, with L_b denoting the length of the observed feedback data sequence and $\mathbf{Z}(n)$ is the *convolution matrix* formed from original TX data sequence $\mathbf{z}(n)$. If least-squares (LS) solution is formed with auto-correlation data windowing method the estimation process gives biased results. Consequently, covariance or pre-windowing methods should be utilized. For covariance method the *convolution matrix* $\mathbf{Z}(n)$ of the original signal is formulated in (6) [7, 8], where N_g denotes the length of estimated imbalance filters $\hat{\mathbf{g}}_1$ and $\hat{\mathbf{g}}_2$.

$$\mathbf{Z}(n) = \begin{bmatrix} z(n-N_g+1) & \cdot & \cdot & z(n) \\ \cdot & & & \cdot \\ \cdot & & & \cdot \\ z(n-L_b+1) & \cdot & \cdot & z(n-L_b-N_g) \end{bmatrix} \quad (6)$$

Corresponding observed feedback data sequence is $\mathbf{y}(n) = [y(n-N_g+1)\ y(n-N_g)\ \cdots\ y(n-L_b+1)]^T$. The minimum phase imbalance filter coefficients $\tilde{\mathbf{g}}_1$ and $\tilde{\mathbf{g}}_2$ best describing the data in the LS sense can be then solved from

$$\begin{bmatrix}\hat{\mathbf{g}}_1 \\ \hat{\mathbf{g}}_2\end{bmatrix} = \mathbf{Z}_b^+(n)\mathbf{y}(n). \quad (7)$$

In (7) $\mathbf{Z}_b^+(n) = (\mathbf{Z}_b^H(n)\mathbf{Z}_b(n))^{-1}\mathbf{Z}_b^H(n)$ is the *pseudo-inverse* of $\mathbf{Z}_b(n)$. Finally the PD filter coefficients can be solved from equation

$$\hat{\mathbf{w}} = -(\hat{\mathbf{G}}_1^H\hat{\mathbf{G}}_1)^{-1}\hat{\mathbf{G}}_1^H\hat{\mathbf{g}}_2^0, \quad (8)$$

where $\hat{\mathbf{G}}_1^H$ is *convolution matrix* formed from $\hat{\mathbf{g}}_1$, and $\hat{\mathbf{g}}_2^0 = [\hat{\mathbf{g}}_2^T 0 \cdots 0]^T$ is a *zero-padded* version of $\hat{\mathbf{g}}_2$ with $N_g - 1$ additional zeros. PD filter $\mathbf{w}$ can be truncated to length N_w, where $1 \le N_w \le N_g$.

3.2 Recursive Least-Squares Approach

Recursive LS (RLS) follows the LS principle but it does not execute matrix inversions which makes it computationally more efficient than plain LS. Recursion has been implemented through *matrix inversion lemma* which gives tools to create matrix inversions in recursive manner. Following RLS formulation corresponds to above block LS with covariance data windowing: [8]

$$\mathbf{k}(n) = \frac{\lambda^{-1}\mathbf{P}(n-1)\mathbf{u}(n)}{1+\lambda^{-1}\mathbf{u}^H(n)\mathbf{P}(n-1)\mathbf{u}(n)} \quad (9)$$

$$e(n) = y(n) - \hat{\mathbf{g}}^H(n-1)\mathbf{u}(n) \quad (10)$$

$$\hat{\mathbf{g}}(n) = \hat{\mathbf{g}}(n-1)\mathbf{k}(n)e^*(n) \quad (11)$$

$$\mathbf{P}(n) = \lambda^{-1}\mathbf{P}(n-1) - \lambda^{-1}\mathbf{k}(n)\mathbf{u}^H(n)\mathbf{P}(n-1) \quad (12)$$

where, $\mathbf{u}(n) = [z(n)\ z(n-1)\ \cdots\ z(n-N+1)\ z^*(n)\ z^*(n-1)\ \cdots\ z^*(n-N+1)]$, $\mathbf{P}(0) = \delta^{-1}\mathbf{I}$ and $\hat{\mathbf{g}}(0) = \mathbf{0}$. δ is small positive constant to ensure non-singularity of the inverse $\mathbf{P}(n)$ of the covariance matrix formed from the original signal.

From estimated imbalance vectors $\hat{\mathbf{g}}$ we get $\hat{\mathbf{g}}_1 = [\hat{\mathbf{g}}(0)\ \cdots\ \hat{\mathbf{g}}(N_g-1)]^T$ and $\hat{\mathbf{g}}_2 = [\hat{\mathbf{g}}(N_g)\ \cdots\ \hat{\mathbf{g}}(2N_g-1)]^T$. Moreover, *zero-padded* versions $\hat{\mathbf{g}}_1^0$ and $\hat{\mathbf{g}}_2^0$ are $\hat{\mathbf{g}}_1^0 = [0\ 0\ \cdots\ \hat{\mathbf{g}}_1^T]^T$ and $\hat{\mathbf{g}}_2^0 = -[0\ 0\ \cdots\ \hat{\mathbf{g}}_2^T]^T$ both with $N_g - 1$ appended zeros. After this PD filter coefficients $\hat{\mathbf{w}}(n)$ are solved again with recursive calculations

compared to (8), basically in a similar manner as the estimation of $\hat{\mathbf{g}}$. Only differences are that equation (10) is changed to

$$e(n) = \hat{\mathbf{g}}_2^0(n) - \hat{\mathbf{w}}^H(n-1)\mathbf{u}(n), \tag{13}$$

where $\mathbf{u}(n) = [\hat{\mathbf{g}}_1^0(n)\ \hat{\mathbf{g}}_1^0(n-1)\ \cdots\ \hat{\mathbf{g}}_1^0(n-N_g+1)]$ and equation (11) is getting the form

$$\hat{\mathbf{w}}(n) = \hat{\mathbf{w}}(n-1)\mathbf{k}(n)e^*(n). \tag{14}$$

Again, PD filter impulse response $\hat{\mathbf{w}}$ can be truncated to the length N_w.

4. PRACTICAL ASPECTS

There are a number of implementation related issues which have to be taken into account to attain maximum performance for the algorithm. Namely, carrier frequency offset (CFO), delay between FBL signal and original signal, FBL signal-to-noise ratio (SNR) and computational complexity of different adaptive algorithms. In this section, other adaptive algorithms found in the literature are considered aside of the RLS algorithm because it is computationally rather complex and performance of the other algorithms have been compared to it. All Matlab simulations are based on frequency-selective I/Q imbalance model with impulse response of length 3, where total amplitude response varies between 0.978 and 1.071, and total phase response varies between 1 and 7 degrees. Moreover, signal with 16-QAM modulation, 35 % roll-off, 5 times over-sampling, 1 MHz symbol rate, 5 MHz sampling frequency, and 1.275 MHz IF has been used. 100 independent simulation runs have been ran for each simulation.

4.1 CFO

First of all, CFO of the FBL signal has to be within certain limits. This requirement should be trivial to fulfill even with free-running LO because frequency source is usually common for up- and down-conversion. For additional info on frequency synchronization see e.g. [9]. The basic impact how FBL CFO affects the average (integrated) IRR on the whole TX band can be seen in Fig. 2. From the figure it can be seen that CFO must be lower than 200Hz to achieve 60 dB IRR. It is also worth noticing that Gauss-Newton RLS (GN) [8] algorithm outperforms other adaptive algorithms when considering FBL CFO.

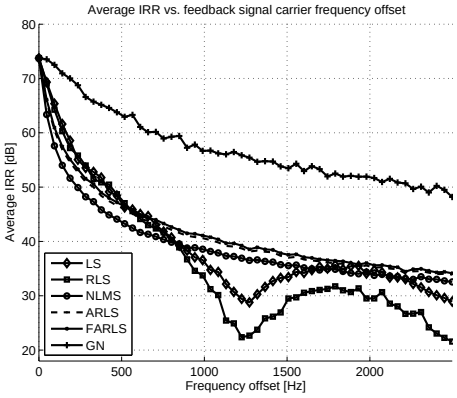

Figure 2: Average IRR as a function of carrier frequency offset. 25,000 samples used for I/Q imbalance parameter estimation.

4.2 Delay Compensation

Another, more paramount requirement is delay estimation and compensation between original digital TX signal and digital FBL signal. Integer delay is easily estimated and compensated but estimation and compensation of fractional-delay (FD) has been found to be more demanding. Moreover, I/Q imbalance tends to bias FD estimates which makes the compensation even more demanding. The effect of FD between original signal and FBL signal on the IRR can be seen in Fig. 3 where performance of different algorithms practically coincide. It can be seen that FD has significant effect on the performance of the algorithm and residual FD less than 1.1 % gives over 60 dB IRR. In addition, 1 % accuracy should be achievable with algorihtms found in the literature, see e.g. [9].

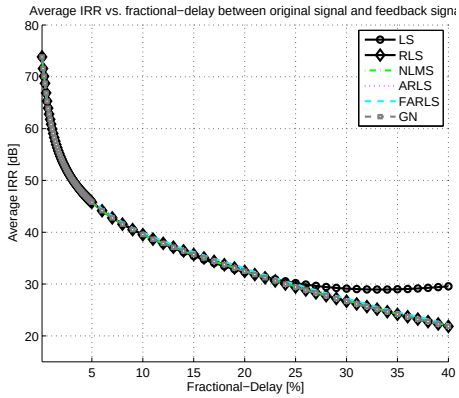

Figure 3: Average IRR as a function of fractional-delay between original signal and FBL signal. 25,000 samples used for I/Q imbalance parameter estimation.

On the other hand, it has been discussed in [7] that with long enough imbalance filters $\hat{\mathbf{g}}_1$ and $\hat{\mathbf{g}}_2$ the FD can be tolerated to some extent without separate FD compensation. In this paper, it is shown that longer imbalance filters indeed relax FD compensation requirements. To achieve this, the assumption of imbalance filters $\hat{\mathbf{g}}_1$ and $\hat{\mathbf{g}}_2$ being minimum phase has to be relaxed and delay to them has to be introduced. However, utilization of longer imbalance filters requires higher FBL SNR. Comparison of IRR with different imbalance filter lengths, and corresponding delays, can be seen in Fig. 4. The optimum delay is always $D = \lfloor (N_g - 1)/2 \rfloor$. From the Fig. 4, it can be clearly seen that algorithm performance between integer delay multiples is significantly improved, and it can tolerate FD to some extent without performance degradation.

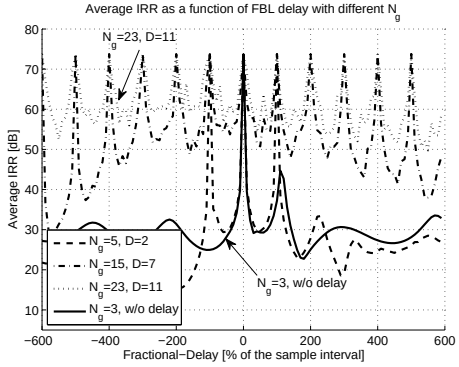

Figure 4: Average IRR with different filter lengths and delays as a function of delay between FBL signal and original signal. 25,000 samples used for I/Q imbalance parameter estimation.

4.3 Feedback loop SNR

Number of samples used for the estimation has also influence on the performance. From the Fig. 5 it can be seen that the SNR of the FBL signal should be over 30 dB to keep the performance degradation due to feedback noise negligible with the reasonable block

lengths discussed here. Fixed PD length results in a saturation of the IRR in Fig. 5. Longer PD lengths result in higher IRR. In the real-time implementation of this paper SNR of the FBL signal in the implementation is around 35 dB. The SNR level was examined offline from received FBL signal.

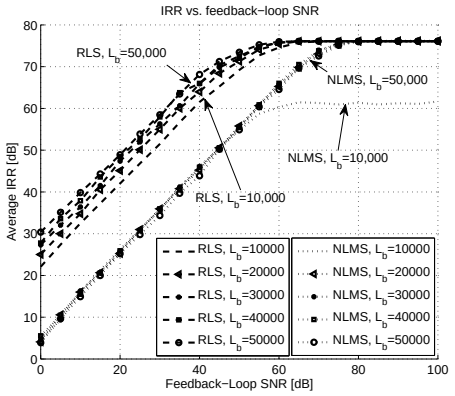

Figure 5: Average IRR with different parameter estimation lengths as a function of SNR of the FBL signal.

4.4 Computational complexity

Computational complexity of different adaptive algorithms is also a very important aspect of the implementation because computation power is always limited and computational burden should be kept as low as possible. In Fig. 6 it can be seen that RLS and GN are clearly the most complex algorithms that have been considered. Approximate RLS (ARLS) [10] and Fast Approximate RLS (FARLS) [11] have complexity close to the normalized least mean squares (NLMS) and their performance is very good if problems discussed above have been solved properly. On the other hand, RLS and GN algorithms outperform other algorithms under more demanding conditions.

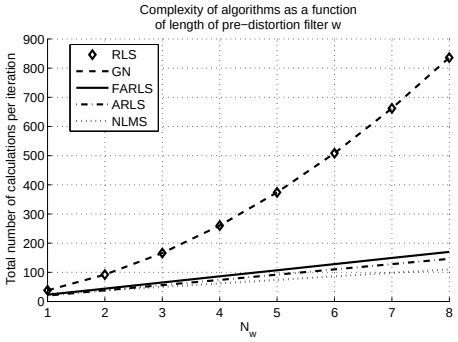

Figure 6: Computational complexity of adaptive algorithms as a function PD filter length. N_g is of same length as N_w.

5. REAL-TIME IMPLEMENTATION PLATFORM

The development environment for the real-time prototype implementation consists of personal computer (PC), software defined radio (SDR) evaluation board and radio-frequency (RF) daughter board. In this work, the evaluation board is Universal Software Radio Peripheral (USRP). The USRP together with daughter board and PC construct a fully functional transceiver unit. In addition, this transceiver unit is definable with computer software, namely GNU Radio [12, 13].

5.1 USRP and RFX2400

USRP is a SDR platform developed by Ettus Research. The USRP platform is based on field programmable gate array (FPGA) and it provides analog-to-digital converters (ADC), DACs, decimating/interpolating low-pass filters, and PC connectivity [13]. Furthermore, it can be used as a low-IF or direct-conversion transceiver which makes it especially suitable for performance measurement of the implemented algorithm. USRP is connected to the PC with universal serial bus (USB) 2.0 interface which limits, in practice, the Rx/Tx bandwidth to 4 MHz.

In the implementation here, the RFX2400 transceiver daughter board (DB) is used. It can operate from 2.3 to 2.7 GHz and has maximum transmission power of 17 dBm [13]. The DB has two RF antenna connections, one for half-duplex transmit and receive called RX/TX and another for receiving called RX2. If RX/TX connection is used for transmitting and RX2 for receiving, the DB is capable of full-duplex data transmission. The RFX2400 has already fairly good IRR figure of about 38 dB but still insufficient for future wireless systems. Block diagram of the RFX2400 can be seen in Fig. 7.

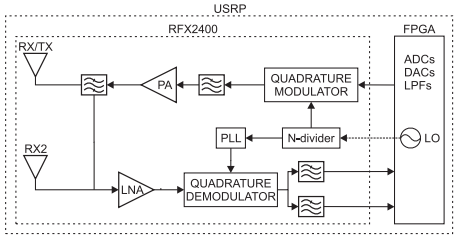

Figure 7: Block diagram of RFX2400 DB and main connections to USRP.

5.2 GNU Radio

GNU Radio (GR) is an open-source software running on Linux operating system which can be used with multiple hardware platforms from a sound card to sophisticated (SDR) platforms, like USRP. Although GR supports multiple platforms, it is mainly intended to be used with the USRP. GR has also been built and installed on Mac OS X. Similarly, there has been attempts to install GR on Microsoft Windows, but successes have not been reported so far [12].

Python flow graphs act as a framework for GR applications. They consist of signal sources, signal processing blocks and signal sinks. Though, signals in GR are discrete time signals, they are processed in block wise manner [14]. GR includes large variety of built-in signal processing blocks. All signal processing blocks are written in C++ or Python programming languages [12, 15]. C++ programming language is considerably more efficient than Python and it has much better ability to execute computationally complex calculations. As a result, blocks with elaborate functionality are programmed in C++ language [16].

6. IMPLEMENTATION AND MEASUREMENT EXAMPLES

RX/TX antenna connection of the RFX2400 was used as a RF output and RX2 antenna connection as FBL RF FE. Physical connections of the implementation can be seen more clearly in block diagram of Fig. 8. Implementation was built on GR software by writing C++ signal processing blocks (SPB) for FBL signal synchronization, I/Q imbalance estimation and PD. Additionally, own interfaces to USRP were written to get better controllability of digital IF and to enable real downconversion in FBL. Also GR Companion (GRC) graphical user interface (GUI) blocks were written for programmed SPBs to get easier usability of overall transceiver. Arbitrary 16-QAM data sequence was generated on-line in each measurement made with prototype implementation.

In the implementation, the accuracy of TX and FBL RX oscillator signals are very good (in the order of 100 Hz), and thus no additional CFO mitigation is here implemented. Integer delay estimation was performed with fast FT (FFT)-based correlator and FD was estimated with non-data-aided (NDA) Maximum Likelihood (ML) algorithm found in [9]. Additionally, the performance of the NDA ML synchronization algorithm was improved with simple interpolating polynomial fitting approach.

Integer delay was compensated by changing vector indexing and FD was compensated with look-up-table (LUT)-based FD filtering. The LUT includes 100 all-pass FD filters of order 32 generated off-line, thus giving an accuracy of 1 % of the sample interval for the compensation. For further information about FD filters, see e.g [17]. Integer delay compensation does not increase computational complexity but FD compensation needs additional 32 multiplications and summations for each output sample. Block diagram of the main implementation DSP functionalities can be seen in Fig. 8. Moreover, RLS parameters for I/Q imbalance estimation in the measurements have been $\lambda = 1$ and $\delta = 0.01$.

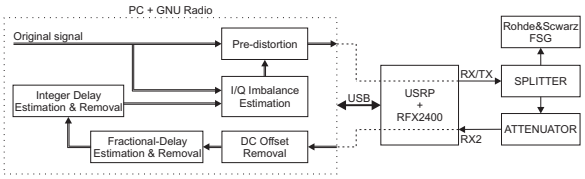

Figure 8: Block diagram of the measurement setup where connections and signal flow can be seen.

Measured spectra are obtained and saved with Rohde&Schwarz FSG spectrum analyzer with measurement setup seen in Fig. 8. In Fig. 9 are USRP output spectra with different PD lengths. Finite image rejection of I/Q mixer on RFX2400 can be seen as rather strong mirror image at 2455 MHz. The performance of the I/Q imbalance mitigation on low-IF signal is very good for all PD lengths. Spectrum plot show over 55 dB average IIR figure which can be considered sufficient for future flexible transceivers. Note that the spike at 2456 MHz is due to the LO leakage of the TX which could be compensated with PD [18] but it has not been considered here. Lower performance of the PD with 2 and 3 taps could be explained with estimation noise due to the FBL SNR, phase noise, residual time synchronization errors or other impairments which have not been taken into account.

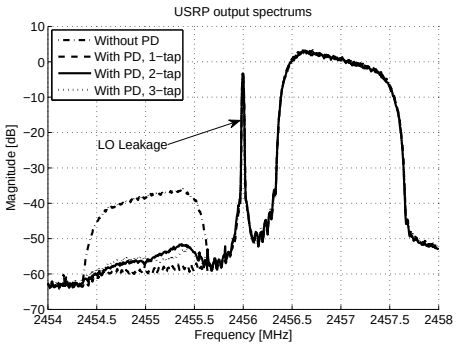

Figure 9: Output spectrum of USRP without and with I/Q imbalance calibration algorithm. Signal with 16-QAM modulation, 1 MHz symbol rate, 1 MHz TX IF, 4 MHZ RX IF, 35 % roll-off, 4 times over-sampling. PD lengths 1, 2 and 3, and 25,000 samples used for estimation.

7. CONCLUSIONS

This article focuses on complex I/Q up-conversion based TX architectures and especially the I/Q imbalance problem in them. An efficient digital PD based imbalance calibration method was presented, with most focus on prototype implementation related aspects and corresponding calibration performance evaluations.

The estimation algorithm and PD structure discussed was shown to be implementable with rather feasible computational resources and it was shown to offer excellent calibration performance. The reliability of the estimation algorithm is practically dependent on the exact delay compensation which was proved to be a demanding task. This prototype implementation gives good basis on future research and work to realize possible FPGA based solutions. Future work will also include real-time prototype implementation of joint PA nonlinearity and I/Q imbalance mitigation algorithm [18].

REFERENCES

[1] S. Mirabbasi, and K. Martin, "Classical and modern receiver architectures," *IEEE Commun. Mag.*, vol. 38, pp. 132-139, Nov. 2000.

[2] P-I. Mak, S-P. U, and R.P. Martins, "Transceiver architecture selection: review, state-of-the-art survey and case study," *IEEE Circuits Syst. Mag.*, vol. 7, pp. 6-25, Apr. 2007.

[3] G. Fettweis, M. Lhning, D. Petrovic, M. Windisch, P. Zillman, and W. Rave, "Dirty RF: a new paradigm," *IEEE Pers. Ind. and Mobile Radio Commun.*, vol. 4, pp. 2347-2355, Sept. 2005.

[4] G. Fettweis, E. Zimmermann, V. Jungnickel, and E.A. Jorswieck, "Challenges in future short range wireless systems," *IEEE Veh. Commun. Mag.*, vol. 1, iss. 2, pp. 24-31, 2006.

[5] Y. Zou, "Analysis and mitigation of I/Q imbalances in multi-antenna transmission systems," Ph.D. dissertation, Tampere University of Technology, Tampere, Finland, 2009.

[6] M. Valkama, "Advanced I/Q signal processing for wideband receivers: models and algorithms," Ph.D. dissertation, Tampere University of Technology, Tampere, Finland, 2001.

[7] L. Anttila, M. Valkama, and M. Renfors, "Frequency-selective I/Q mismatch calibration for wideband direct conversion transmitters," *IEEE Trans. Circuits Syst.*, vol. 55, pp. 359-363, Apr. 2008.

[8] S. Haykin, *Adaptive Filter Theory*, 3^{rd} ed. Prentice Hall, 1996.

[9] U. Mengali, and A.N. D'Andrea, *Synchronization Techniques for Digital Receivers*, Plenum Press, 1997.

[10] M.M. Chansarkar, U.B. Desai, and B.V. Rao, "A comparative study of the approximate RLS with LMS and RLS algorithms," *Fourth IEEE Region 10 Int. Conf., TENCON '89*. pp. 255-258, Now. 1989.

[11] M.M. Chansarkar, and U.B. Desai, "A fast approximate RLS algorithm," *IEEE Conf. on Computer, Communication, Control and Power Engineering*, vol.3, pp. 532-536, Oct. 1993.

[12] GNU Radio, Accessible: http://www.gnuradio.org/.

[13] Ettus Research, Accessible: http://www.ettus.com/.

[14] N. Manicka, "GNU Radio Testbed," M.Sc. Thesis, University of Delaware, USA, 2007.

[15] A.M. Wyglinski, M. Nekovee, and Y.T.Hou, *Cognitive Radio Communications and Networks*. Elsevier Inc., 2010.

[16] E. Blossom, "How to write a signal processing block," Accessible: http://www.gnu.org/software/gnuradio/doc/howto-write-a-block.html.

[17] T.I. Laakso, V. Välimäki, M. Karjalainen, and U.K. Laine, "Splitting the unit delay," *IEEE Signal Process. Mag.*, vol. 13, iss. 1, pp. 30-60, Jan. 1996.

[18] L. Anttila, P. Händel, and M. Valkama, "Joint mitigation of power amplifier and I/Q modulator impairments in broadband direct-conversion transmitters," *IEEE Trans. Microw. Theory Tech.*, vol. 58, iss. 4, pp. 730-739, Apr. 2010.